Available online at www.sciencedirect.com
SCIENCE DIRECT®
Cement & Concrete Composites 28 (2006) 564–571
Cement & Concrete Composites
www.elsevier.com/locate/cemconcomp

Analytical evaluation of pull-out tests—The inverse problem

B. Banholzer [a,*], W. Brameshuber [a], W. Jung [b]

[a] Institute of Building Materials Research at RWTH Aachen University (ibac), Schinkelstrasse 3, 52062 Aachen, Germany
[b] Institute for Pure and Applied Mathematics at RWTH Aachen University (iram), 52062 Aachen, Germany

Received 10 March 2004; accepted 13 February 2006
Available online 4 April 2006

Abstract

A numerical solution routine is proposed, which provides a simple and straightforward analytical method to evaluate the prevailing bond characteristics of a composite by means of a bond stress versus slip relation $\tau(s)$ using experimental data from pull-out tests. Time consuming and sometimes nonconvergent optimization procedures which have been used so far to determine $\tau(s)$ can be avoided. The proposed solution routine is applied and validated using experimental data from pull-out tests which were carried out at steel fiber/concrete systems. It is also shown that the underlying bond stress versus slip relation $\tau(s)$ is a material parameter, since it is not dependent on geometric factors of fiber and matrix, for example fiber diameter and embedded length.

Keywords: Pull-out test; Cohesive interface model; Simulation; Inverse problem

1. Introduction

The structural performance of a composite is strongly affected by the properties of the fiber/matrix interface. However there are currently no straightforward experimental methods to determine these interface properties, because of the difficulties involved in conducting strain measurements on short thin fibers. Nevertheless many different alternative test set-ups and experimental techniques have been developed in recent years to gain more insight into the basic mechanisms dominating the properties of the fiber/matrix interface. One of the most popular is the pull-out test in which a single fiber or bar is pulled out off the surrounding matrix and the corresponding load versus displacement relation, $P(\omega)$, is recorded. However, the resistance P to the debonding and pull-out processes depends on the bond properties of the fiber/matrix interface and the interfacial bond area, as a function of the length of the embedded fibers and fiber diameter. Hence, the $P(\omega)$ is a characteristic only for the tested geometric arrangement and does not represent a material specific relation of the tested composite. In order to yield material parameters, which generally define the shear force transmission between the fiber and the matrix and are independent of the geometric arrangement, mathematical models have to be applied to analyze the experimentally determined $P(\omega)$ relation. Many of these models use systems of equations to analytically describe the processes occurring in a pull-out test, and a so called bond stress versus slip relation (BSR), $\tau(s)$, to define the interfacial material properties [10,4]. This analysis consists of a primal problem (*direct boundary value problem*) whereby a given BSR is used to simulate a load versus displacement relation $P(\omega)$, and a secondary problem in which the BSR is obtained from an experimental pull-out curve (*inverse boundary value problem*). Until today, all proposed models are based in common on the direct boundary value problem. Only in combination with an optimization algorithm, which fits the simulated pull-out curve to the experimental data by adapting the BSR, it is so far possible to actually derive the unknown functional relationship $\tau(s)$ for a fiber/matrix combination. However, even with modern numerical optimization routines, it is quite a difficult task to derive this functional relationship if $\tau(s)$ is a complex function defined by many parameters. Therefore the

* Corresponding author. Fax: +49 (0) 241 809 2139.
E-mail address: Banholzer@ibac.rwth-aachen.de (B. Banholzer).

0958-9465/$ - see front matter © 2006 Elsevier Ltd. All rights reserved.
doi:10.1016/j.cemconcomp.2006.02.015

models linking the interface shear stress, τ, to the relative displacement (i.e. the slip, s) are usually limited to a small number of parameters, and thus an unrestricted functional description of the interface properties is impossible. This will cause a substantial effect on the accuracy of the simulated pull-out response, if the interfacial properties predominating the real structure cannot be described accurately by the approximation of the BSR $\tau(s)$.

Based on the work of the previous paper [1] regarding the direct boundary value problem (primal problem), an analytical solution procedure for the straightforward inverse determination of the BSR from experimental test results is presented in this study (secondary problem). An analytical model is derived to allow the calculation of an N-piecewise linear bond stress versus slip relation $\tau(s)$ with no limitation of N using an experimentally determined load displacement distribution $P(\omega)$. In comparison to other inverse numerical approaches known from the literatures, no fitting and optimization processes are needed anymore and, in addition, the number of functional parameters defining the BSR $\tau(s)$ is not initially limited. To illustrate the mathematical background, demonstrate the applicability, and carry out a validation of the proposed model, the BSR $\tau(s)$ is obtained from experimental pull-out curves $P(\omega)$ recorded during pull-out tests of steel fiber/concrete systems with different geometric arrangements. Since the performed simulations can predict the experimental pull-out responses fairly well, and independently of the specified geometric arrangements, the BSR $\tau(s)$ is found to be a material property defining the interfacial characteristics between fiber and matrix.

2. The inverse boundary value problem

It is found and shown in [1] that a straightforward relation between the BSR $\tau(s)$ and the corresponding pull-out force $P(\omega)$ exists. Thus it is possible not only to obtain a load versus displacement relation from a given bond stress versus slip relation, but also to derive a bond stress versus slip relation from a given load versus displacement relation that is $P(\omega) \rightarrow \tau(s)$ for a given $P(\omega)$. Consequently, the slip distribution over the embedded length $s(x)$ is defined as presented in [1] for the direct boundary value problem. Here, the axial coordinate, x, is $0 \leqslant x \leqslant L$ where as the L is the embedded length of the fiber in the matrix. Instead of determining the pull-out force P_n in an iterative procedure, the shear stress τ_n is identified for different load steps n. From the experimental pull-out test the fiber displacement of load applied end (ω_n) and the corresponding pull-out force P_n are known for each load step (see Fig. 2 for illustration). From [1] it was found that φ is the normalized pull-out force and γ is sum of the inverse extensional stiffness of fiber and matrix respectively as

$$\gamma = \frac{1}{A_F E_F} + \frac{1}{A_M E_M} \tag{1}$$

A_F and A_M are the load carrying areas of the fiber and matrix, and E_F and E_M are the moduli of elasticity of the fiber and the matrix respectively. To allow an unrestricted mathematical description of the bond law, an N-piecewise linear relation (N is not limited) between the bond stress τ and the slip s is used as shown in Fig. 1 and is normalized for simplicity in term of $T(s)$ as

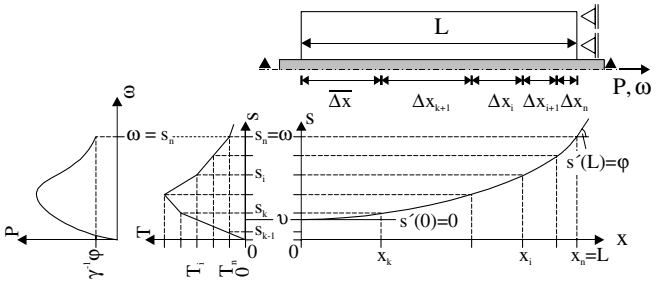

Fig. 1. Slip distribution and boundary conditions at the left and right side of the system.

$$T(s) = m_i(s - s_{i-1}) + T_{i-1} = \pi \mathrm{d} \gamma \tau(s),$$
$$m_i = \frac{T_i - T_{i-1}}{s_i - s_{i-1}}, \quad T_0 = s_0 = 0 \tag{2}$$

(normalized bond stress versus slip relation (NBSR)).

To simplify the following derivation we consider only the load steps $\omega_n = s_n$. Then, ω_n always corresponds to the slip s_n at a location $x_n = L$ as well as to the slip s_n in the $T(s)$ relation and is hence the upper-bound of the interval n of the piecewise linear function $T(s)$, with $0 \leqslant i \leqslant n$. Thereby the normalized pull-out force φ_n corresponds to the slope s'_n at the location $x_n = L$. The slope $s'(x)$ corresponds to the normalized force $q(x) = \gamma F_F(x) = s'(x)$ in the fiber at a given location x (see [1], for more details).

Similar to the routine described in [1], a T_n has to be found in an iterative procedure for a given displacement $\omega = s(x = L)$ and a given pull-out force $P = \gamma^{-1}\varphi = \gamma^{-1}s'(L)$ such that depending on m (see Eq. (2)) the incremental lengths Δx_i, is obtained as

$$\Delta x_i = \frac{1}{\sqrt{m_i}} \ln \left[\frac{\sqrt{m_i} q_i + T_i}{\sqrt{m_i} q_{i-1} + T_{i-1}} \right] \quad \text{for } m_i > 0 \tag{3}$$

and

$$\Delta x_i = \frac{1}{\sqrt{-m_i}} \arcsin \left[\frac{\sqrt{-m_i}(T_i q_{i-1} - T_{i-1} q_i)}{T_{i-1}^2 - m_i q_{i-1}^2} \right] \quad \text{for } m_i < 0. \tag{4}$$

Thus the embedded length L can be defined as

$$L \overset{!}{=} \overline{\Delta x} + \sum_{i=k+1}^{n} \Delta x_i \tag{5}$$

where $\overline{\Delta x}$ is (see Fig. 1)

$$\overline{\Delta x} = \frac{1}{\sqrt{m_k}} \ln \left[\frac{\sqrt{m_k} q_k + T_k}{\sqrt{T_k^2 - m_k q_k^2}} \right], \quad m_k > 0$$

$$\overline{\Delta x} = \frac{1}{\sqrt{-m_k}} \arcsin \left[\frac{\sqrt{-m_k}(-q_k \sqrt{T_k^2 - m_k q_k^2})}{T_k^2 - m_k q_k^2} \right], \quad m_k < 0 \tag{6}$$

The lower-bound k in Eqs. (5) and (6) is equal to the interval i at which the force in the fiber turns zero. It can be evaluated by using

$$q_{i-1}^2 = q_i^2 - m_i(s_i - s_{i-1})^2 - 2\,T_{i-1}(s_i - s_{i-1}) \tag{7}$$

in a recursive manner from $i = n(\varphi_n = q_n)$ with a decreasing step until $(q_{k-1})^2 < 0$ is satisfied. The point (s_n, T_n) and hence the point (s_n, τ_n) of the wanted BSR are found, if the boundary condition $s'(0) = 0$ of the original BVP and hence Eq. (5) are satisfied (compare Eqs. (1)–(3) in [1]).

Starting at a very early load level and therefore with a small initial displacement ω_1 and assuming a piecewise linear relation between T and s, the corresponding and only unknown variable is T_1 which can easily be determined with Eq. (5), knowing that $m_1 > 0$ and $n = 1$ (see Fig. 2). Hence, the first point in the BSR is found.

Choosing a following load step and a somewhat higher displacement ω_2 (hence $n = 2$ now), T_2 can be evaluated in a similar iterative procedure using Eq. (7) in a recursive manner from $i = n = 2$ $(\varphi_2 = q_2)$ until $(q_{k1})^2 < 0$ is determined. Then the interval number k in Eq. (5) in which the force in the fiber turns zero is found. If the chosen T_2 further satisfies Eq. (5), the next point in the NBSR is evaluated (see Fig. 2). Note that for this recursive calculation the already known part of the NBSR is needed. Similar to the above described procedure the total NBSR can now be evaluated with load step by load step. This method is a kind of collocation since $\varphi(\omega)$ is defined at points $\omega = s_0, \ldots, s_n$. It is simple because only one value T_n is evaluated at each step.

In contrast to the direct boundary value problem a problem arises from this stepwise determination of the NBSR because, as mentioned above, all previous identified linear parts of the NBSR are needed for the determination of a further point i in the $T(s)$ relation. For the direct boundary value the identified pull-out forces at a certain load step are no longer used in the further calculation and errors made during the evaluation of this parameter do not influence the further calculation of the load displacement curve. However, for the inverse boundary value problem, every single point (s_i, T_i) for $k \leqslant i \leqslant n$ of the normalized bond law ascertained before is needed to identify a

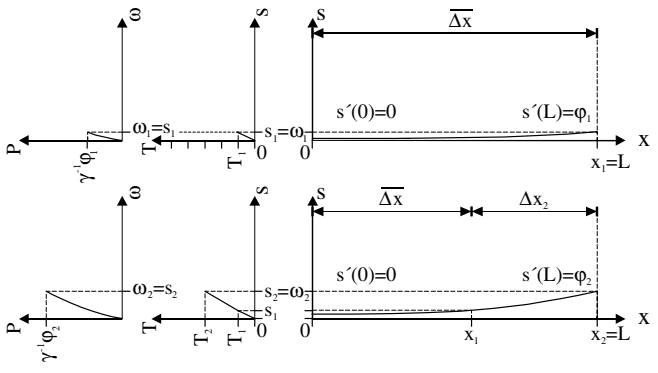

Fig. 2. Inverse determination of $T(s)$.

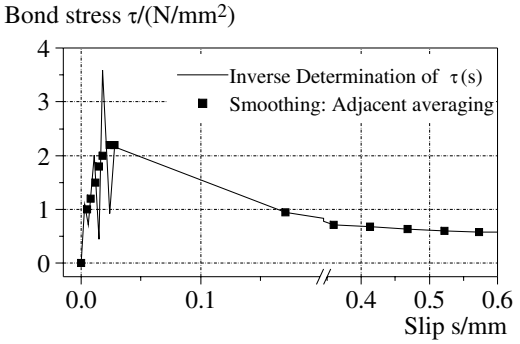

Fig. 3. Oscillation effects during the identification of $T(s)$.

further point (s_n, T_n) of the wanted NBSR. Therefore the errors made in the derivation before do sum up or even potentially grow that results in oscillation effects and in the worst case in a diverging calculation (see Fig. 3 for an example). This phenomena was observed in many cases for inverse boundary value problems and for different applications before. For a general overview on inverse problems in engineering mechanics see [12,13].

To minimize the influence of this error propagation, certain features and regularization methods were implemented in the numerical solution routine developed during this study. Among other things, the collocation method is modified to include a forward regularization technique similar to [9].Thus the afore mentioned oscillation and error magnification effects are reduced to a considerable degree. Another possibility is the implementation of a monotonicity condition, that is after evaluation of the maximum normalized bond stress T_{cr} in the NBSR, the values T_n must be determined such that $T(s)$ is monotonously decreasing.

On basis of the model presented here it is now possible to derive a normalized bond stress versus slip relation $T(s)$ and hence the actual bond stress versus slip relation $\tau(s)$ from the experimental result of a pull-out test $P(\omega)$ in a straightforward way without using any optimization routines or fitting procedures. To show the application of the algorithm and allow a validation of the cohesive interface model, the pull-out tests on steel fiber/cement based matrix systems with different fiber diameters and embedded lengths are carried out and evaluated in regard to the underlying BSR.

3. Experiments

In principle, the single fiber pull-out test is based on a relatively simple experimental configuration and has been widely used to investigate the shear bond properties not only of steel fiber or re-bar/cement based matrix systems (e.g. [10,11]) but of ceramic matrix (e.g. [3]) and polymer matrix composites (e.g. [14]) as well. However, this experimental technique has some limitations associated with the scale of the test. Firstly, there is a maximum embedded length of the reinforcing element, L_{crit}, permitting the pull-out without a tensile failure of fibers. Secondly, the

stochastic size effects can be observed for fibers of small diameters embedded in a cement based matrix, as this matrix is an inhomogeneous structure [8]. Thus the random arrangement of pores, for example, can induce a dramatically decreasing of the effective embedded length not visible from the outside. This effect will in turn result in an underestimation of the actual shear bond properties if it is not accounted for in the analytical model used for the evaluation. Nevertheless, if these aspects are considered during the testing procedure and later on during the analytical evaluation process, the single fiber pull-out test is an applicable tool to investigate the shear bond properties.

3.1. Materials composition and specimen preparation

The straight and smooth steel fibers with different diameters are cast in a fine grained concrete matrix (PZ-0899-01), which features a maximum grain size of 0.6 mm, a water/binder ratio of 0.4, and a binder content of 700 kg/m^3. For more information refer to [7]. During the casting, the fibers are situated vertically in the mold of dimension 50 mm × 50 mm × L, with L being the embedded length of the fiber. The fibers run over the total height of the specimen and extend on the upper side about 125 mm and on the lower side about 50 mm. The hole on the lower side of the mold allowing the fiber to extend is sealed with silicon paste. The embedded length L is varied from 12.1 to 80.0 mm and the fiber diameter from 0.3 to 2.5 mm (Table 1). All fibers used in the test are previously degreased with aceton. After casting the specimens are compacted for 60 sec. on a V-B table with a vibration amplitude of 0.5 mm. The specimens are cured in the mold for 48 hours and then stored at 20 °C and 65% RH until testing at a total age of 7 days. In tensional tests, the Young's modulus of the fine grained concrete was determined to be 35,000 N/mm^2 [6] and of the steel fiber to be 210,000 N/mm^2, respectively.

Table 1
Combinations of fiber diameter and embedded length of fiber tested

Combination	Fiber diameter, d/mm	Embedded length, L/mm
1	2.5	35.0
2	2.0	40.0
3	**2.0**	**35.0**
4	2.0	30.0
5	2.0	20.0
6	2.0	10.0
7	1.5	80.0
8	1.5	30.0
9	**1.5**	**27.1**
10	1.2	27.1
11	1.0	30.0
12	1.0	22.1
13	**0.8**	**22.1**
14	0.6	30.0
15	0.6	17.1
16	0.3	30.0
17	0.3	13.6
18	0.3	12.1

3.2. Experimental sequences

The experimental program carried out in this investigation to verify the cohesive interface model and to study the interfacial bond in cement based composites comprises a total of 18 series of tests. Each series is arranged with five replications for a certain combination of fiber diameter and embedded length. These combinations are specified in Table 1. For the sake of clarity, only the results of the highlighted combinations are listed in the following and the results of remaining combinations are presented in [2].

3.3. Experimental methods

In order to examine the debonding and pull-out processes in the experiments, the specimen is glued at its bottom side to a steel block, such that the fiber extends through a hole, and its end is attached to a linear variable differential transducer (LVDT), fixed to the bench of the universal testing machine (Instron 5566) (see Fig. 4 for a schematic illustration of the test set-up). The steel block itself is also fixed by a frame to the bench of the testing machine, and the top end of the fiber is clamped by a mechanical grip at a free length of 100 mm to the crosshead of the Instron. The loading is controlled by crosshead displacement with a rate of about 0.10 mm/min. This deformation control is adopted to allow measurement in the residual stage. If the cross head displacement is utilized to gain information on the deformation of the fiber right atop the matrix, the elastic strain contribution over the free length of the steel fiber between the clamping and the point of intersection with the matrix has to be subtracted. To avoid the problems, which result from this manual revision of the $P(\omega)$ relation, e.g. due to a slip in the mechanical clamping, a video extensometer is used in this study.

This system consists of two main parts: a video camera and a video processing part, which is stored in a PC containing a frame-grabber interface card and software to analyze the data. The frame-grabber card converts the PAL video signal into an 8-bit digital format whilst simultaneously generating an 800 × 600 pixel image. The interface is capable of resolving the gray scale level of each pixel in 256 shades. An analogue interface is available to connect the load cell (Instron, measuring range 0.1–5.0 kN) to the PC and hence allows both signals to be saved simultaneously. The video-extensometer operates directly as a (non-contact) displacement measurement device by determining the change in distance between two markers, the so-called targets. The targets produce rapid contrast changes in gray scale and thus allow the evaluation of the absolute displacements of a point by tracking these specific gray scale distributions in the x- and y-direction, respectively, in the sequence of the pictures taken (12.5 pictures per second). The maximal resolution depends on the field of view. In the present case the accuracy is determined for a display window of 10 × 10 mm^2, which is utilized for the testing, as about 0.6 μm. Two white paint markings,

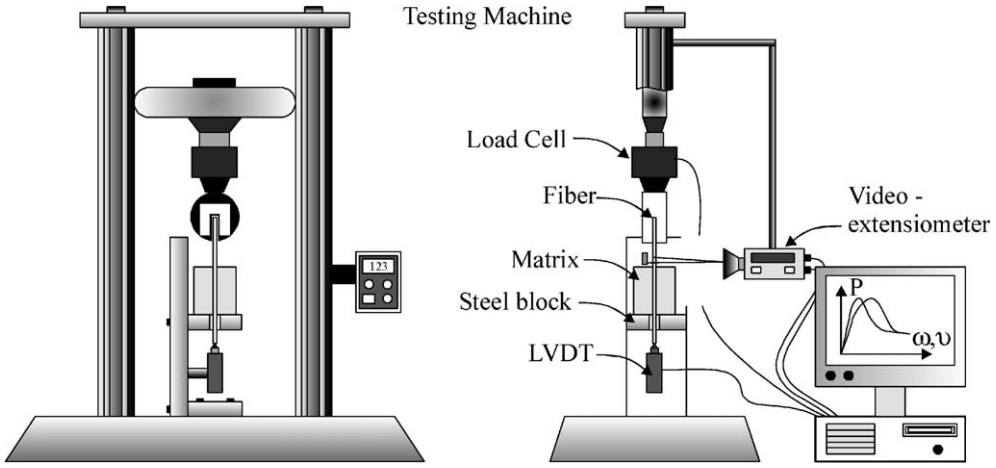

Fig. 4. Setup for pull-out tests on steel fibers embedded in a cement based matrix.

one on the steel fiber itself about 0.1 mm above the intersection point of fiber and matrix and another on a reference plate fixed to the bench, are used as targets for the video extensometer.

Hence, instrumentation is provided to measure the displacement of the fiber at the active (loaded) and passive (free) end relative to the end faces of the specimen, i.e. $P(\omega)$ and $P(\upsilon)$ relations are obtained at the loaded and free fiber end, respectively. The applied force, and the displacements of the loaded as well as free end of the fiber are continuously recorded for every 2 N change in force.

3.4. Test results

The load displacement curves are given separately for the loaded as well as for the free fiber end displacements, that is $P(\omega)$ in Figs. 5–7 and $P(\upsilon)$ in Figs. 8–10, respectively (black lines). Additionally, in each diagram the corresponding simulated $P(\omega)$ or $P(\upsilon)$ curves are plotted (black squares). As it will be explained later in this study, these simulated load deflection curves are based on one and the same BSR $\tau(s)$, which is evaluated with the numerical implementation of the cohesive interface model.

All of the listed experimental results show the typical and expected process found in pull-out tests. An increasing part governed by elastic bond, followed by a decreasing softening branch and finally by a fade out controlled by friction. Because the fiber is pulled through the surrounding matrix, the frictional bond resistance stays constant although some minor changes can be detected possibly on account of abrasion effects or wedged aggregates. The variation of the load deflection curves is dependent on the fiber diameter and embedded length used in the test.

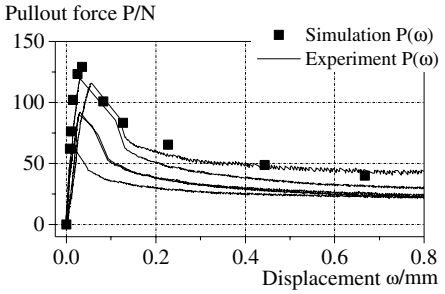

Fig. 5. Load versus active fiber end displacement diagram $P(\omega)$, for a steel fiber diameter of 0.8 mm and an embedded length of 22.1 mm (combination 13 in Table 1).

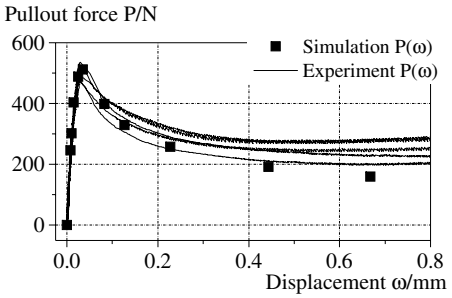

Fig. 6. Load versus active fiber end displacement diagram $P(\omega)$, for a steel fiber diameter of 2.0 mm and an embedded length of 35.0 mm (combination 3 in Table 1).

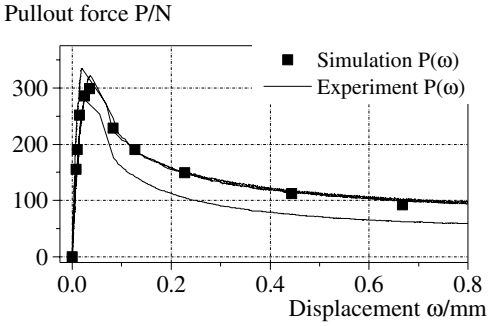

Fig. 7. Load versus active fiber end displacement diagram $P(\omega)$, for a steel fiber diameter of 1.5 mm and an embedded length of 27.1 mm (combination 9 in Table 1).

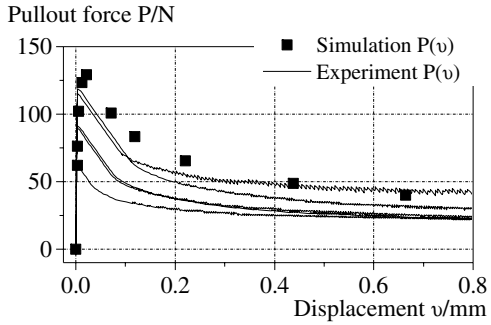

Fig. 8. Load versus passive fiber end displacement diagram $P(\upsilon)$, for a steel fiber diameter of 0.8 mm and an embedded length of 22.1 mm (combination 13 in Table 1).

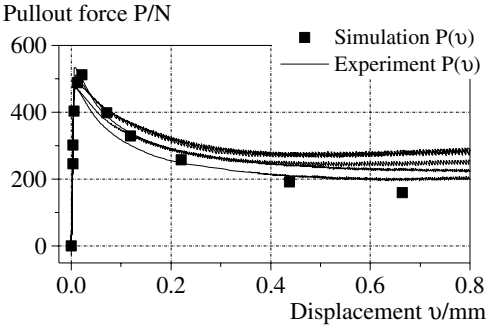

Fig. 9. Load versus passive fiber end displacement diagram $P(\upsilon)$, for a steel fiber diameter of 2.0 mm and an embedded length of 35.0 mm (combination 3 in Table 1).

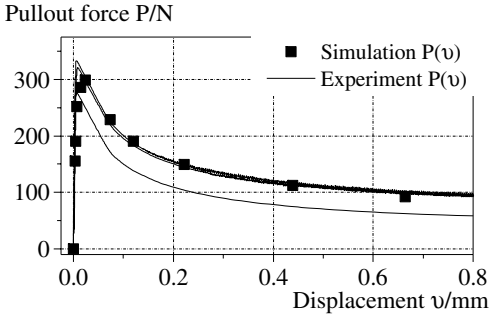

Fig. 10. Load versus passive fiber end displacement diagram $P(\upsilon)$, for a steel fiber diameter of 1.5 mm and an embedded length of 27.1 mm (combination 9 in Table 1).

With increasing fiber diameter and/or embedded length the scatter decreases. It may be stated here, that the test results of the remaining combinations listed in [2] show the same characteristics. A more detailed investigation (probabilistic approach) of the large variation of the test results is also given there.

4. Application of the model

The derivation of the above described model is based on a pull-push test, that is a fiber is pulled out of the matrix against a restraint, in contrast to the experimental tests presented, which are pull-pull tests (the matrix is restrained at the rear). However, as has been shown in [15,5] the influence of a different loading condition on the expected results can be neglected, if the ratio between the stiffness of the fiber and that of the matrix is greater than 10, that is $E_M A_M / E_F A_F \geqslant 10$. In the present case the extensional stiffness of the fiber is found to be e.g. for a fiber diameter of 2 mm

$$E_F A_F = 210{,}000\ \mathrm{N/mm^2} \cdot \frac{\pi 2^2}{4}\ \mathrm{mm^2} \cong 660\ \mathrm{kN}$$

The Young's modulus of the fine-grained concrete is determined to be 35,000 N/mm^2, however the load carrying area of the matrix is not known. Pure expertise states that not the whole cross sectional area of 50×50 mm^2 will contribute to the load transmission. Nevertheless, own experimental tests carried out using fiber optic strain sensors, which are embedded in the matrix at different radial distances from the fiber, showed that the load carrying area is large enough to guarantee, that an extensional stiffness ratio greater than 10 is maintained. Hence, the proposed solution routine is not only valid for a pull-push test but also for a pull-pull test in which a fiber is pulled out of or pulled through the matrix, which is restrained at its rear.

Applying this routine for the evaluation of the load displacement curves $P(\omega)$ presented in Figs. 5–7 and in [2], the underlying BSR $\tau(s)$ can be evaluated for each test separately. Exemplary the derived $\tau(s)$ curve for one pull-out test of a 0.8 mm diameter steel fiber embedded over 22.1 mm in fine grained concrete (combination 13 in Table 1) is listed in Fig. 3; note the oscillations.

If a subsequent averaging technique is adopted to smooth the oscillations of the BSR (black squares in Fig. 3) and the presented routine is used for all 5 test results of combination13 in Table 1, the BSR listed in Fig. 11 can be obtained. The bond laws of the investigated test series show variations corresponding to those of the $P(\omega)$ relations, see Fig. 5. The black squares in Fig. 11 refer to the calculated average BSR of combination 13.

If, for all combinations listed in Table 1 and all replications of tests within a series, the underlying average bond

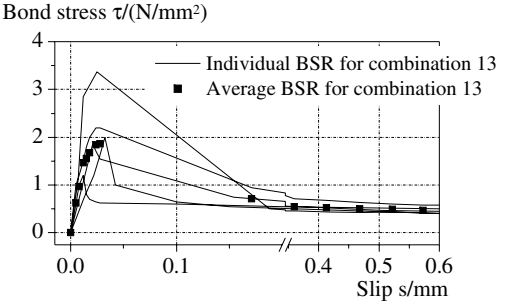

Fig. 11. Evaluated bond stress versus slip relations $\tau(s)$ for all tests of combination 13 in Table 1 (0.8 mm fiber diameter and an embedded length of 22.1 mm, steel fiber/fine grained concrete (PZ-0899-01) system).

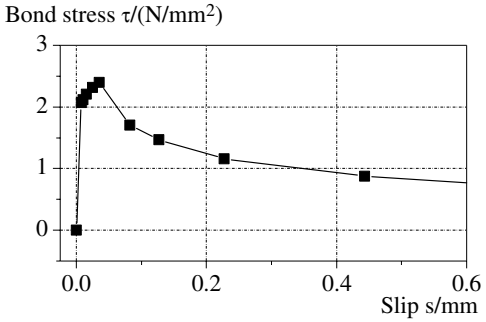

Fig. 12. Evaluated bond stress versus slip relation $\tau(s)$ for the material combination steel fiber/fine grained concrete (PZ-0502-01).

law is derived and a weighted averaging technique is used, an overall average BSR $\tau(s)$ can be evaluated as presented in Fig. 12. On basis of this evaluated $\tau(s)$ relation, the direct boundary value problem is used to simulate the expected pull-out response for the different fiber diameters and embedded lengths tested. The results of these simulations are shown in Figs. 5–7 together with the experimental pull-out test results. In general it may be stated that a good consistency with the experimental tests is achieved.

These results show that the proposed cohesive interface model is capable of simulating the pull-out processes of fibers embedded in a cement based matrix. As the simulated $P(v)$ relations (Figs. 8–10, load versus fiber end displacement) are only used for validation, they additionally state the principal validity of the proposed model. Furthermore, due to their good agreement with the measured $P(v)$ relations it is also proven that the evaluated $\tau(s)$ relation can be seen as a material parameter which characterizes the bond between a steel fiber and the fine-grained concrete independent of any geometric properties.

5. Summary and conclusions

An analytical evaluation procedure for a pull-out test is proposed in the present study. It is based on an inverse boundary problem and allows the straightforward calculation of an N-piecewise linear bond law $\tau(s)$ with no limitation of N, on basis of an experimentally determined load displacement distribution $P(\omega)$.

The presented model is applied and validated using experimental results of pull-out tests, carried out on smooth and straight steel fiber/fine grained concrete systems. It is found that the determined bond stress versus slip relation $\tau(s)$ is a material parameter, since it is not dependent on geometric factors of fiber and matrix, for example fiber diameter and embedded length. However, experimental tests that have not been published in this study showed so-called stochastic size effects [2]. That is if the fiber diameter is small in regard to the maximum grain size used in the cement based matrix, the pull-out behavior is influenced more significantly in the post failure region due to, for example, abrasion effects.

Nevertheless, bond characteristics of different fiber/matrix systems can be compared much more in detail with the presented model because the complete bond stress versus slip relation is known. Furthermore, only if $\tau(s)$ is known, a tailoring of the interface properties in regard to an optimized mechanical performance of the composite material with enhanced characteristics is possible. In future work, different effects due to, for example, lateral pressure on the fiber, constant loading, and repeated load cycles, will be considered. It is also possible to extend this model to deformed fibers (which is the 'norm' these days) by considering additional frictional effects due to the deformation of the fibers within the $\tau(s)$ relation.

Acknowledgement

This project is part of the Collaborative Research Center 532 "Textile reinforced concrete—basics for the development of a new technology" and sponsored by the Deutsche Forschungsgemeinschaft (DFG). The support is gratefully acknowledged.

References

[1] Banholzer B, Brameshuber W, Jung W. Analytical simulation of pull-out-tests—the direct problem. Cement and Concrete Composites 2005;27(1):93–101.
[2] Banholzer B. "Bond Behaviour of a Multi-Filament Yarn Embedded in a Cementious Matrix". In: Schriftenreihe Aachener Beiträge zur Bauforschung, Institut für Bauforschung der RWTH Aachen, 12, (pdf file at: http://www.bth.rwth-aachen.de), 2004.
[3] Barsoum M, Tung IC. Effect of oxidation on single fiber interfacial shear stresses in SiC–borosilicate glass systems. J Amer Ceram Soc 1991;74:2693–6.
[4] Bazant ZP, Desmorat R. Size effect in fiber or bar pull-out with interface softening slip. J Eng Mech 1994;120(9):1945–63.
[5] Brameshuber W, Banholzer B, Brümmer G. Ansatz für eine vereinfachte Auswertung von Faser-Ausziehversuchen. Beton- und Stahlbeton 2000;95(12):702–6.
[6] Brameshuber W, Brockmann T. Betonformulierung – Methodik und Stoffgesetze. Aachen: Rheinisch-Westfälische Technische Hochschule. In: SFB 532: Textilbewehrter Beton – Grundlagen für die Entwicklung einer neuartigen Technologie, Arbeits- und Ergebnisbericht 2. Hj '99-'01, 2.Hj.'02, 2002. p. 195–233.
[7] Brockmann T. Anforderungen und Eigenschaften zementgebundener Feinbetone. Aachen: Lehrstuhl und Institut für Massivbau. In: in Aachen Hegger, J. (editor), Textilbeton. 1. Fachkolloquium der Sonderforschungsbereiche 528 und 532, 15. und 16. Februar 2001, 2001. p. 82–98.
[8] Gutiérrez MA, Borst de R. Deterministic and stochastic analysis of size effects and damage evolution in quasi-brittle materials. Arch Appl Mech 1999;69:655–76.
[9] Lamm PK. A survey of regularization methods for first-kind Volterra equations. In: Colton D, Engl HW, Louis A, McLaughlin JR, Rundell W, editors. Surveys on solution methods for inverse problems. Vienna, New York: Springer; 2000. p. 53–82.
[10] Naaman AE, Najm H. Bond-slip mechanisms of steel fibers in concrete. ACI Mater J 1991;88(2):135–45.
[11] Somayaji S, Shah SP. Bond stress versus slip relationship and cracking response of tension members. ACI Mater J 1981;78(1):217–225.
[12] Tanaka M, Dulikravich DS. ISIP 1998: inverse problems in engineering mechanics. In: International symposium on inverse

problems in engineering mechanics 1998 (ISIP '98), Nagano, Japan. Amsterdam: Elsevier; 1998.
[13] Tanaka M, Dulikravich DS. ISIP 2000: inverse problems in engineering mechanics II. In: International symposium on inverse problems in engineering mechanics 2000 (ISIP 2000), Nagano, Japan. Amsterdam: Elsevier; 2000.
[14] Zhandarov S, Pisanova E, Mäder E. Is there any contradiction between the stress and energy failure criteria in micromechanical tests? Part II: Crack propagation: effect of friction on force–displacement curves. Compos Interf 2000;7(3):149–75.
[15] Zhou L-M, Kim J-K, Mai Y-W. On the single fibre pull-out problem: effect of loading method. Compos Sci Technol 1992;45:153–60.